Discover Energy

Research

Optimizing Organic Rankine Cycle (ORC) configurations integrated with transient industrial waste heat: a multi-objective approach

Yohan Engineer[1,2] · Ahmed Rezk[1,2] · Mahmoud B. Elsheniti[3] · Ehsan Baniasadi[1,2] · Ahmed Fouly[3]

Received: 28 June 2024 / Accepted: 21 October 2024
Published online: 07 November 2024

Abstract

Decarbonizing heat-intensive industries by reusing the waste heat for power or combined heat and power systems is becoming increasingly important to address global warming. The Organic Rankine Cycle has shown a high level of feasibility and performed efficiently for utilizing medium-to-low-grade heat from renewable resources and heat-intensive industries for direct power generation. This study contributes to the field by conducting a techno-economic investigation of various Organic Rankine Cycle configurations to enhance energy conversion when real-life transient waste heat sources are available. These configurations were optimized to maximize energy output along with economic benefits. The non-linear programming by quadratic Lagrangian, a computational unintensive yet accurate optimization algorithm, was utilized for the multi-objective optimization. The optimized cycle configurations showed a 12.57% enhancement of turbine efficiency. Combining regeneration and recuperation enhanced the superheating by 32%, and the optimized air preheater cycle improved the overall objective by 64.2% compared to the pre-optimized conventional cycle, leading to a feasible 1.72-year payback period.

Keywords Organic Rankine Cycle · Transient waste heat · Multi-objectives optimization · Variable expander efficiency · Economic benefits

Abbreviations

CEPCI	Chemical engineering plant cost index
GA	Genetic algorithm
KKT	Karush–Kuhn–Tucker
LCOF	Levelised cost of fuel
LMTD	Logarithmic mean temperature difference
NLPQL	Non-Linear Programming by Quadratic Lagrangian
ORC	Organic Rankine Cycle
RANS	Reynolds-averaged Navier–Stokes
SIC	Specific investment cost
WHR	Waste heat recovery

✉ Ahmed Rezk, a.rezk@aston.ac.uk | [1]Energy and Bioproducts Research Institute (EBRI), College of Engineering and Physical Science, Aston University, Birmingham B4 7ET, UK. [2]Mechanical, Biomedical and Design Engineering Department (MBDE), College of Engineering and Physical Science, Aston University, Birmingham B4 7ET, UK. [3]Mechanical Engineering Department, College of Engineering, King Saud University, 11451 Riyadh, Saudi Arabia.

List of Symbols

$€H_{recovery}$	Thermal energy value (€)
$€H_T$	Electricity generation value (€)
A	Area (m2)
C	Cost (€)
C_p	Specific heat (kJ/kg K)
F	Mean temperature correction factor (–)
G	Turbine Loss coefficient (–)
h	Specific enthalpy (kJ/kg)
htr	Heat transfer coefficient (–)
LF	Dry flue gas heat loss fraction (–)
MP	Mean Power (kW)
$\dot{m}$	Mass flow rate (kg/sec)
N	Rotational speed (RPM)
$Power$	Work done by turbine (kW)
P	Pressure (Bar)
$\dot{Q}$	Heat flow rate (kW)
ΔT_{lm}	Logarithmic mean temperature difference (–)
T	Temperature (°C)
U_0	Overall Heat transfer coefficient (W/m^2 K)
$\dot{V}$	Specific Volume (m^3/kg)
Vol	Volume (m^3)
$\dot{W}$	Work done (kW)

Subscript

APH	Air Pre Heater
B	Blade
CEPD	Condensate Extraction Pump discharge
Cond	Condenser
Eco	Economiser
Evap	Evaporator
HX	Heat Exchanger
N	Nozzle
p	Primary loss
R	Ratio
Recup	Recuperator
REFyear	Reference year
Reg	Regenerator
s	Secondary loss
SH	Superheater
TM	Thermal mass
Turb	Turbine
HX	Heat Exchanger

Greek

η	Efficiency
ε	Heat exchanger effectiveness (–)

1 Introduction

Utilizing organic Rankine cycles (ORCs) for employing renewable and waste heat has been extensively researched [1, 2]. ORCs are prevailing in solar-based combined heat and power systems [3, 4]. They are also suitable for harnessing renewable heat sources like geothermal energy [5, 6]. ORCs for waste heat recovery (WHR-ORCs) have proven their practicality in industrial various settings, such as casting plant, cement plants, and smelting furnaces [7, 8]. These applications are critical given the escalating energy costs and environmental considerations [9]. ORCs are adaptable, capable of operating at lower pressures, and well-suited for fluctuating waste heat sources [10]. However, the widespread adoption of WHR-ORCs is hindered by their high initial investment and the need for more affordable components.

Park et al. [11] found that previous experimental research on small-scale WHR-ORCs employing reused expanders, and despite their availability and suitability for use by ORCs, there has been limited exploration of industrial applications. ORCs have been prevailing in metal and cement and plants, because of their compatibility with stable high-grade waste heat [12]. With respect to process industries, 50–66% of their energy input being wasted in a form medium- to low-grade (200–50 °C) [13]. Up to 22% of heat is lost in the stack into the environment at 140–200 °C in Sub-critical industrial boilers, which utilize fossils, biomass and refuse-derived fuels (RDF) [14]. Such a wasted energy causing significant thermal pollution and contribution to the carbon footprint [15], presenting an opportunity for WHR-ORC utilization [16].

Axial flow turbines are widely accepted as the preferred expander for ORC applications with gross power generation > 20 kWe because of their scalability, efficiency, fixed internal leakages, rotational speed, off-design flexibility, simplicity, proven industrial track record, ease of availability, low acquisition cost, low maintenance cost and linear torque spread across a rotation [17].

Enhancing energy conversion efficiency by utilizing recuperation and regeneration schemes along with using different working fluids has been widely studied [18]. For instance, recuperated-superheater in ORCs was found enhancing the overall cycle efficiency when utilizing zeotropic mixtures [19]. On the other hand, LeCompte et al. [10] observed that the additional pressure drop by integrating the recuperation to an unconstrained waste heat stream outweighed its heat recovery benefits and increased capital cost, limiting sensible heat recovery potential [20]. The regeneration was found to enhance the ORC's overall efficiency by increasing the high-pressure turbine's mass flow and reducing condenser heat rejection [21]. Despite decreasing the power output, Xi et al. [22] discovered that the regeneration process decreased the boiler evaporation load, improved the exergetic cycle efficiency, and enhanced the thermodynamic performance under Genetic Algorithm-optimized operating conditions [22], agreeing with Mago et al. [23]. Accordingly, optimal flow was nearly 20% of the total flow by Battista et al. [24]. A study conducted by Roumpedakis et al. [25] highlighted the importance of thermal and economic multi-objective optimization for WHR ORCs that utilized the Genetic Algorithm approach. However, the Genetic Algorithm is computationally extensive. Therefore, Hu et al. [26] compared Genetic Algorithm to the Nonlinear Programming by Quadratic Lagrangian (NLPQL) for diesel engines' optimization, which concluded the suitability of NLPQL for multi-objective optimization with better computational effectiveness compared to the former.

The waste heat from industrial steam boilers might be utilized as a source for low-grade organic Rankine cycle (WHR-ORC) recovery. However, this potential has not been scrutinized. The heat from steam boilers is readily available in established industries and implementing WHR-ORC technology can rapidly improve the energy sustainability of these industries. Previous research on WHR-ORCs utilizing flue gas emphasized steady heat sources and assumed fixed isentropic turbine efficiency along with omitting pressure drop in the heat exchangers [27]. Moreover, the fluid could only operate in the saturated phase. Exploring the thermo-economic impact of using an actual transient heat source to power an ORC is a computationally intensive process that has not been fully comprehended. Whereas combined thermodynamic and thermo-economic multi-objective optimization for increasing overall output and exergetic efficiencies have been applied to other energy recovery systems, they have not been applied to waste heat recovery based ORCs yet [28, 29].

This work aims to perform multi-objective optimization for the sizes of components in Organic Rankine Cycles (ORCs), considering various cycle configurations with the impact of maximizing the ORCs' power output while utilizing a finite transient waste heat and minimizing their specific investment costs. The novelty of this work lies in (i) undertaking a parametric study for a broad range of cycles employing realistic transient heat source available in numerous industries (i.e., industrial steam boiler-based cycle-level transient), benchmark their performance and optimise their designs thermo-economically; (ii) introducing NLPQL as computationally less intensive multi-objective optimisation than other computationally intensive evolutionary techniques; (iii) consider the realistic variable turbine efficiency using turbine loss models in the multi-objective optimisation. Accordingly, the objectives of this study are to (i) develop a thermodynamic for the several ORC integrations coupled with Craig and Cox loss turbine models to capture the change in the turbine efficiency during operation; (ii) optimize the component sizes of ORC configurations using NLPQL optimization to minimize the fuel consumption and maximize the energy efficiency; (iii) undertake techno-economic assessment and

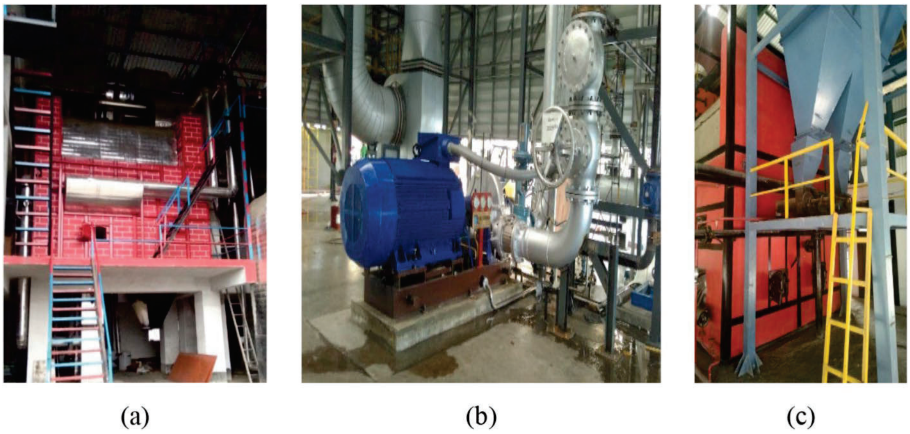

Fig. 1 **a** The boiler **b** steam turbine **c** coal screw feeders

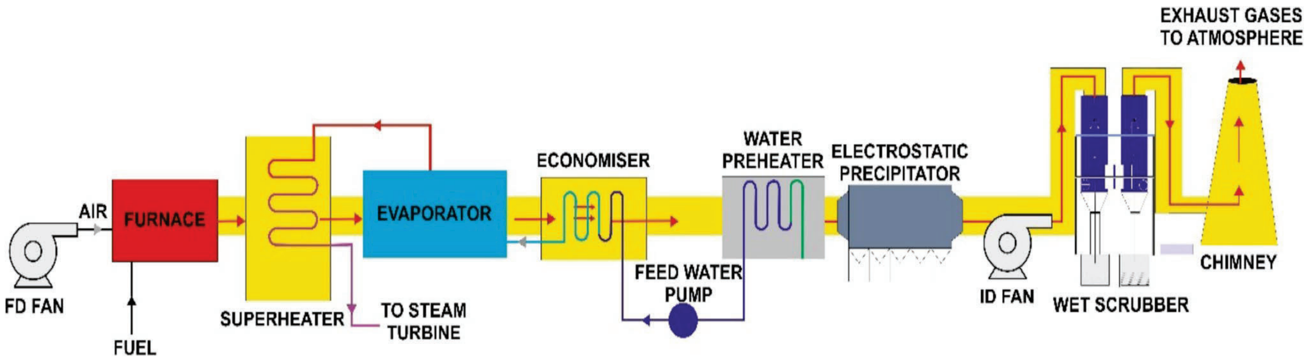

Fig. 2 Steam boiler flue gas path

determine the payback of advanced cycle configurations compared to conventional ORC, utilizing flue gas waste heat from an exemplar industrial steam boiler.

2 Materials and methods

2.1 Heat source

The transient heat source profiles were derived from the waste heat of a chimney linked to a steam boiler, depicted in Fig. 1a. This boiler is installed in a textile factory in Ghaziabad, India, and the process is illustrated in Fig. 1. The Indonesian sub-bituminous coal fuel is used of 23 MJ/kg calorific value [30]. The steam drives 300 kW incidental cogeneration micro steam turbine and the steam exit at 4 bars for the remaining process.

The combustion airflow system is equipped with forced and induced draft fans to ensure continuous flue gas flow, as illustrated in Fig. 2. A series of counter-current heat exchangers are employed to optimize heat recovery at various points in the system, considering the system's pinch point.

In this system, and according to the manufacturer, 35% excess air above the stoichiometric mixture was utilized, aligning with Widodo et al. and Mastral et al. [31, 32], which utilized fluidised bed combustion boilers. The flue gas mass flow rate and the system's corresponding input energy were determined, as shown in Fig. 3. Table 1 shows operating conditions samples in 8 h shift.

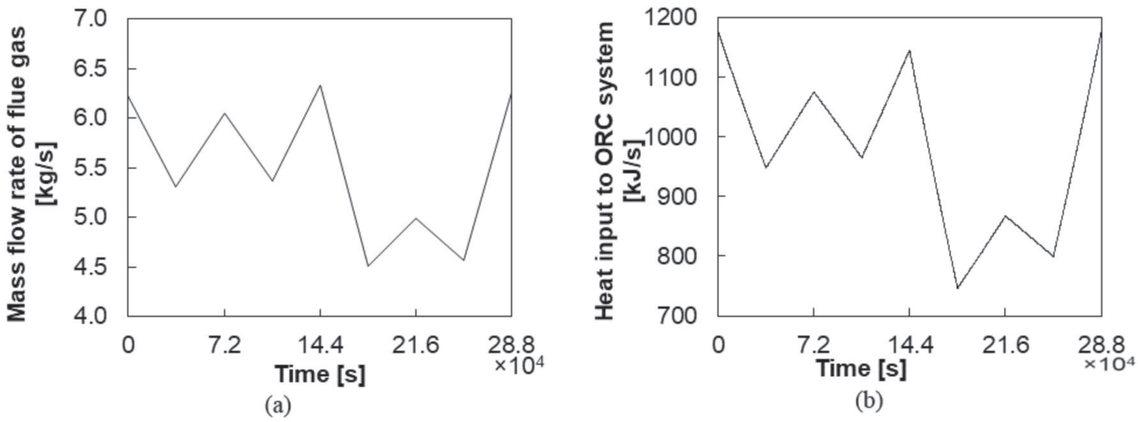

Fig. 3 **a** Flue gas flow rate **b** corresponding energy input (i.e., heat source) to ORC system from the flue gas

Table 1 Flue gas parameters

Time of day	Steam flow	Fuel consumed	Fuel input energy	Stoichio-metric air	Total flue gas	Total feed air	Flue gas Tempera-ture	Steam turbine power
hh:mm	kg/s	kg/s	kJ/s	kg/s	kg/s	kg/s	°C	kW
07:30	3.58	0.597	11947.8	4.61	6.23	5.629	181	284
08:30	3.05	0.509	10174.6	3.93	5.30	4.793	177	264
09:30	3.48	0.581	11610.0	4.48	6.05	5.469	176	278
10:30	3.09	0.515	10301.2	3.98	5.37	4.853	178	264
11:30	3.65	0.608	12158.8	4.69	6.34	5.728	179	296
12:30	2.59	0.433	8654.7	3.34	4.51	4.077	164	242
13:30	2.87	0.479	9575.8	3.70	4.99	4.511	172	259
14:30	2.63	0.438	8769.9	3.39	4.57	4.132	173	242
15:30	3.60	0.599	12010.0	4.63	6.26	5.66	181	273

2.2 Organic rankine cycle configurations

This study investigated ten variations of the ORCs using the Simcenter Amesim™ simulation tool. These configurations involved performance enhancing methods like heat storage, direct recuperation, regeneration, and a combination of these approaches. The conventional ORC is depicted in Fig. 4a. Figure 4b shows an ORC with thermal storage by adding three masses of 104 kg each, GS-53 cast iron. Using air preheater to elevate the boiler's feed air temperature is illustrated Fig. 4c. Figure 4d and e illustrate the recuperative cycle and its combination with heat storage, respectively. Figure 4f demonstrates a configuration where the high-temperature exhaust fluid of the turbine is first passed through the recuperator followed by air preheater to maximize the cyclic efficiency. Figure 4g presents an ORC incorporating regenerator operates at intermediate pressure to increase the working fluid's temperature entering the economizer. Figure 4h illustrates ORC incorporating air preheater combined with regeneration, and Fig. 4i illustrates the combination of heat storage and regeneration. Finally, a new configuration combining regeneration and recuperation is shown in Fig. 4j.

Refrigerant R245fa, a commonly used working fluid in commercialized ORC plants, was chosen for this study despite its high GWP index (930). This decision was based on its compatibility with common ORC materials, high thermal stability up to 250 °C, high exergetic efficiency, low evaporation temperature, low specific investment cost, high autoignition temperature of 412 °C and zero ozone-depleting potential. From a thermodynamic perspective,

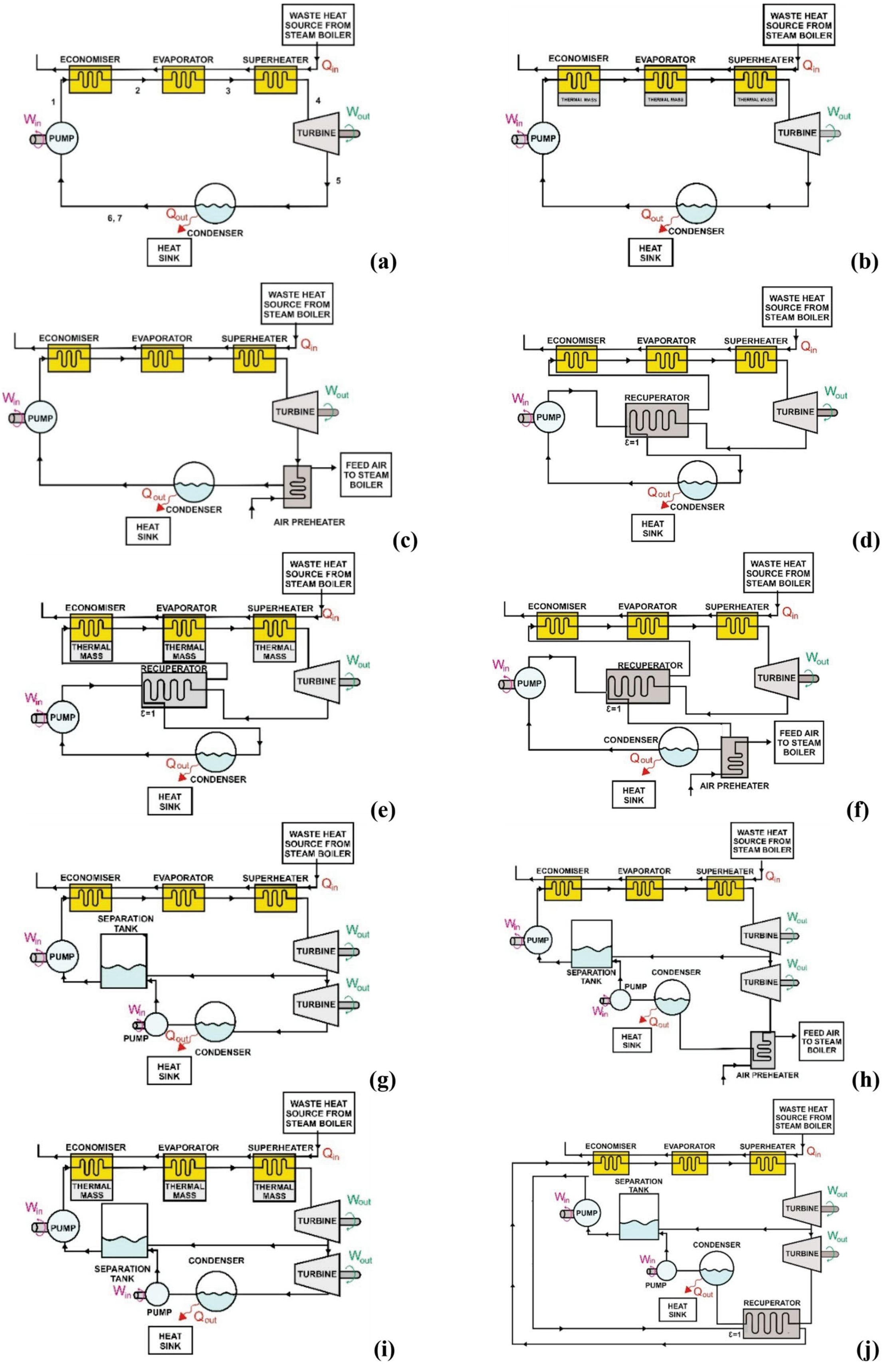

Fig. 4 Schematic layout for ORC configurations **a** Conventional cycle **b** thermal storage **c** air preheating **d** recuperation **e** thermal storage and recuperation **f** air preheating and recuperation **g** regeneration **h** air preheating and regeneration **i** thermal storage and regeneration **j** recuperation and regeneration

R245fa has showed high thermal efficiency and power density for ORCs operating with low-to-medium-temperature heat. The low critical pressure of R245fa allows critical regime operation and reasonable thermal efficiency [33]. However, the turbine size is limited to prevent supersonic flow in the turbine, so a single-stage turbine is the recommended choice. R245fa's dry fluid slope prevents moisture accumulation at the turbine exit. Its above atmospheric condensing pressure eliminates the requirement for an ejector or vacuum system and streamlines turbomachinery shaft sealing.

3 Mathematical modelling

This section presents the governing equations, optimisation approaches and the economic assessments used for assessing the previously introduced ORC configurations. Simcenter Amesim™ simulation tool was utilized for system-level modelling coupled with a turbine model considering its performance variation during the operation and modelled using the Engineering Equation Solver™ sub-programme.

3.1 Thermodynamic analysis

3.1.1 Heat source

Equations 1, 2, 3 show the mass and energy balances for the combusted coal exhaust stream employed to determine the heat input to the investigated ORCs.

$$\dot{m}_{fluegas} + \dot{m}_{ash} = \dot{m}_{st,air} + \dot{m}_{excess,air} + \dot{m}_{fuel} \tag{1}$$

$$LF_{fluegas} = \frac{M_{ratio} C_{p_{fluegas}} \left(T_{fluegas,out} - T_{feed,air}\right)}{GCV_{coal}} \tag{2}$$

$$\dot{Q}_{cycle} = \dot{m}_{fluegas}\left(h_{fluegas,in} - h_{fluegas,out}\right) \tag{3}$$

where, $\dot{m}_{fluegas}$ is the flue gas mass flow rate (kg/s); M_{ratio} the mass of flue gas per unit kg of coal ($kg_{fluegas}/kg_{fuel}$); $\dot{m}_{ash}$ denotes the quantity of produced ash (kg/s); $\dot{m}_{st,air}$ the ideal air flow rate for stoichiometric combustion (kg/s); $\dot{m}_{excess,air}$ denotes the additional air to enhance the combustion (kg/s); $\dot{m}_{fuel}$ denotes the rate of combusted mass of coal (kg/s).

The fractional heat loss because of dry flue gases was determined to quantify the fuel saved by utilizing air preheater (APH) achieved, Eq. 2. $LF_{fluegas}$ is the dimensionless fractional dry flue gas; $C_{p_{fluegas}}$ is the flue gas's specific heat ($kJ/kg_{fluegas}$ K); $T_{fluegas,out}$ is the flue gases' exit temperature; $T_{feed,air}$ denotes the temperature of the ai' flow to the boiler downstream air preheater (APH) (°C); GCV_{coal} den'tes the coal's gross calorific value (kJ/kg_{coal}).

Equation 3 is used to determine the heat-energy balance, where $\dot{Q}$ is the heating power added to the ORC (kW); $h_{fluegas,in}$ denotes the flue gas specific enthalpy upstream the ORC heat exchangers ($kJ/kg_{fluegas}$ K); $h_{fluegas,out}$ is the flue gas specific enthalpy downstream the ORC heat exchangers ($kJ/kg_{fluegas}$ K).

3.1.2 ORC turbine

Integrating the turbine's instantaneous pow'r $\dot{W}_{Turb}$ over a given period (t) determines the mean power (MP_{Turb}) (kW) in Eq. 4.

$$MP_{Turb} = \frac{\int_{t=0}^{t=t_{max}} W_{Turb}\, dt}{Operatingtime} \tag{4}$$

Craig & Cox and Moustapha [34, 35] for design and off-design models, respectively, were employed to determine the turbine efficiencyη_{Turb}. Equations 5 determine the turbine efficiency, which is a function of inlet temperature(T_1), mass flow rate ($\dot{m}$), pressure ratio(P_R), speed(N). It is also a function of several losses: G_{BN}&G_{SB} blade's primary'and secondary losses, G_{PN}&G_{SN} nozzle's primary and s'condary losses [36]. Equation 6 determines the instantaneous ORC efficiency $\left(\eta_{cycle}\right)$.

$$\eta_{\mathrm{Turb}} = f\left(\dot{m}, N, P_{TubIn}, T_1, G_{PN}\, G_{PB}, G_{SN}, G_{SB}\right) \tag{5}$$

$$\eta_{cycle} = \frac{\dot{W}_{Turb} - \dot{W}_{Pumps}}{\dot{Q}_{cycle}} \tag{6}$$

3.1.3 Heat exchangers

The area of heat exchanger (A_{HX}) (m^2) is a function of the operating temperature, working fluids flow conditions, the magnitude of heat transfer ($\dot{Q}_{transfer}$)(kW) and the heat exchanger design, as shown in Eq. 7 [37]. The mean temperature correction factor (F) is heat exchanger design-specific, and the flow conditions influence the overall heat transfer coefficient (U_0) (W/m^2 K). The heat exchangers were considered being made of aluminium and the overall heat transfer coefficient was determined based on the dominated convection heat transfer resistance between the heat exchanger walls and fluids flow in both sides, as in Eq. 8. The convection heat transfer coefficients were determined based on the fluid used, the flow rate and the operating conditions utilising the fluid database in the commercial computational platform (i.e., Simcenter Amesim™).

$$A_{HX} = \frac{\dot{Q}_{transfer}}{U_0 F \Delta T_{lm}} \tag{7}$$

$$\frac{1}{U_0} = \frac{1}{htr_{fluegas}} + \frac{1}{htr_{fluid}} \tag{8}$$

where, htr_{fluid} and $htr_{fluegas}$ are the heat transfer coefficients (W/m^2 K) of the ORC working fluid and flue gas, respectively. In evaporation, Verein Deutscher Ingenieure (VDI) atlas for horizontal tubes correlation was used as it has been validated for modelling two-phase flow for most modern refrigerants. For temperature rise across a single phase, the Nusselt number correlation developed by the Gnielinski, which is the modified Petukhov–Popov equation, for single phase heat transfer across turbulent flow in tubes was used. It is widely accepted for Reynolds number values above 4000, as stated in Eq. 9 below where f_{Dff} is the Darcy friction factor, described by Petukhov and shown in Eq. 10 [38].

$$Nu = \frac{\left(\frac{f_{Dff}}{8}\right)(Re - 1000)Pr}{1 + 12.7\left(\frac{f_{Dff}}{8}\right)\left(Pr^{\frac{2}{3}} - 1\right)} \tag{9}$$

$$f_{Dff} = \left(0.79 \times \ln\left(Re_D\right) - 1.64\right)^{-2} \tag{10}$$

The LMTD for the APH, superheater, economiser, recuperator, and evaporator are subscribed by *APH*, *SH*, *Recup*, *Eco*, and *Evap*, respectively, as per Eqs. 11–13.

$$\mathrm{LMTD}_{Eco}, \mathrm{LMTD}_{Evap}, \mathrm{LMTD}_{SH} = \frac{\left(\left(T_{fluegas,in} - T_{fluid,out}\right) - \left(T_{fluegas,out} - T_{fluid,in}\right)\right)}{\ln\left(\frac{T_{fluegas,in} - T_{fluid,out}}{T_{fluegas,out} - T_{fluid,in}}\right)} \tag{11}$$

$$\mathrm{LMTD}_{Recup} = \frac{\left(\left(T_{Turb,out} - T_{Eco,,fluid,in}\right) - \left(T_{Cond,in} - T_{Pump,out}\right)\right)}{\ln\left(\frac{T_{Turb,out} - T_{Eco,,fluid,in}}{T_{Cond,in} - T_{Pump,out}}\right)} \tag{12}$$

$$\mathrm{LMTD}_{APH} = \frac{\left(\left(T_{APH,fluid,inORCAPHIn} - T_{APH,air,outAFOut}\right) - \left(T_{APH,fluid,outORCAPHOut} - T_{feed,air}\right)\right)}{\ln\left(\frac{T_{APH,fluid,in} - T_{APH,air,out}}{T_{APH,fluid,out} - T_{feed,air}}\right)} \tag{13}$$

where, $T_{fluegas,in}$ and $T_{fluegas,out}$ are the heat exchanger, flue gas inlet and exit temperature; $T_{fluid,in}$ and $T_{fluid,out}$ are the heat exchanger inlet and outlet temperatures of the working fluid in; $T_{Turb,out}$ denotes the fluid temperature at exiting the turbine and flowing to the recuperator; $T_{Cond,in}$ denotes the condenser inlet temperature from the recuperator; $T_{Pump,out}$ denotes the pump to the recuperator fluid temperature; $T_{Eco,fluid,in}$ denotes the recuperator-to-economiser working fluid's temperature; $T_{feed,air}$ denotes the feed air's temperature; $T_{APH,'ir,out}$ denotes the feed air temperature after APH; $T_{A'H,fluid,in}$ denotes the turbine to APH fluid temperature; $T_{APH,fluid,out}$ denotes the APH to condenser fluid temperature. Equations 14, 15 determine the recuperator's effectiveness and energy balance, where, $h_{Eco,fluid,in}$ is the working fluid specific enthalpy (kJ/kg) from'he recuperator to the economiser, from the pump to the recuperator ($h_{Pump,out}$), from the turbine to the recuperator ($h_{Turb,out}$) and from the recuperator to the condenser ($h_{Cond,in}$) [39].

$$\varepsilon_{Recup} = \frac{h_{Eco,fluid,in} - h_{Pump,out}}{h_{Turb,out} - h_{Cond,in}} \tag{14}$$

$$\dot{m}_{Pump,out}\left(h_{Eco,fluid,in} - h_{Pump,out}\right) = \dot{m}_{Turb,out}\left(h_{Turb,outExh} - h_{Cond,in}\right) \tag{15}$$

Equations 16, 17 show the mass and energy balance in the regenerator. MFR_{bleed} denotes the mass flow fraction used for the regeneration process; $\dot{m}_{bleed}$ denotes is the bleed fluid flow rate; h_{bleed} denotes the bleed fluid specific enthalpy; $\dot{m}_{CEPD}$ denotes the condensate extraction pump discharge flow rate; h_{CEPD} denotes the condensate extraction pump discharge specific enthalpy; $h_{LPT,out}$ denotes low-pressure turbine discharge specific enthalpy; $\dot{m}_{Reg,out}$ denotes the regenerator discharge flow rate; $h_{Reg,out}$ denotes the regenerator discharge specific enthalpy.

$$MFR_{bleed} = \frac{h_{Reg,out} - h_{CEPD}}{h_{bleed} - h_{CEPD}} \tag{16}$$

$$\dot{m}_{bleed}h_{bleed} + \dot{m}_{CEPD}h_{CEPD} = \dot{m}_{Reg,out}h_{Reg,out} \tag{17}$$

Equation 18 determines the heat rejection from the condenser ($\dot{Q}_{cond}$).

$$\dot{Q}_{cond} = \dot{m}_{Cond,fluid}\left(h_{Cond,in} - h_{Cond,out}\right) = U_{0,Cond}A_{cond}\Delta T_{lm,Cond} \tag{18}$$

where $h_{Cond,in}$ and $h_{Cond,out}$ are the working fluid specific enthalpies at the condenser inlet and outlet; $U_{0,\mathrm{Cond}}$ denotes the condenser overall heat transfer coefficient; A_{cond} denotes the condenser overall heat transfer area; $\Delta T_{lm,Cond}$ denotes the condenser LMTD. The working fluid properties was modelled using Helmholtz rule of internal energy, as it was the most suitable for considering the change in the fluid's thermodynamic energy across the multi-phase flow [40].

3.2 Economic analysis

Equation 19 calculates the specific investment cost(SIC), which includes both capital investment and labor cost, in relation to the economic benefits derived from the generated electricity and heat recovery [41]. In the equation, $₠H_{recovery}$ represents the generated electricity cost, while $₠H_{recovery}$ symbolizing the value of recovered heat, considering the levelized cost of fuel (LCOF) for coal. This is closely linked to the fuel savings resulting from the increased air temperature the steam boiler provides by the air pre-heater.

The costs for components and labour are detailed in Table 2. 34.78 € per kilogram was the working fluid's cost [25]. The average global cost in 2023 was used to determine the cost of the thermal mass made of cast iron [42]. Accordingly, Eq. 20 determines the total capital cost.$Mass_{Thermal}$,$Mass_{fluid}$,Vol_{tank}, and $C_{capital}$ represent the heat storage mass, the working fluid mass, its volume stored between the pump and condenser, and the overall capital expenditure. L_{pipe} and D_{pipe} and denote the pipes' length and diameter, which are determined'o maintain the fluid pressure drop 0.02 bar/m-length according to the Mac-Adams correlation. $\dot{W}_{Pump}$ and MP_{Pump} represent the pump's specific work done and the energy consumption, respectively. These values are furnished in Table 3.

Table 2 Component and labour costs

Component	Component cost equation	References
Turbine	$1.5 \times (225 + 170 \times \dot{V}_{in})$	Quoilin and Declaye [43]
Heat exchangers	$190 + 310 \times (A_{Eco} + A_{Evap} + A_{SH} + A_{Cond} + A_{Recup} + A_{APH})$	Quoilin and Declaye [43] Roumpedakis et al. [25]
Feed pump	$900 \times \left(\frac{\dot{W}_{Pump} \times MP_{Pump}}{300} \right)$	Lecompte and Huisseune [44]
Storage tank	$31.5 + 16 \times Vol_{tank})$	Quoilin and Declaye [43]
Working fluid	$34.08 \times Mass_{fluid}$	Roumpedakis et al. [25]
Piping	$(0.89 + 0.28 \times D_{pipe}) \times L_{pipe}$	Lecompte and Huisseune [44]
Thermal mass	$0.25 \times Mass_{Thermal}$	Golubev et al. [42]
Miscellaneous	300	Kavvadias and Quoilin [45]
Installation labour	$0.3 \times C_{capital}$	Quoilin and Declaye [43] Roumpedakis et al. [25]

Table 3 Diameter and length of working fluid piping

Section of piping	Diameter (mm)	Length (m)
Pump to economiser	50	3
Superheater to turbine	80	5
Turbine to condenser	800	6
Condenser to pump	50	10
Recuperator piping on liquid side	50	3
Recuperator piping on vapour side	800	3
Regenerator bleed	3	5

$$SIC = \frac{C_{Components} + C_{Labour}}{\dot{W}_T + \dot{H}_{recovery}} \tag{19}$$

$$C_{Components} = C_{Pump} + c_{Eco} + C_{Evap} + C_{SH} + C_{Turb} + C_{Cond} + C_{Piping} + C_{fluid} + C_{Recup} + C_{Reg} + C_{APH} + C_{TM} \tag{20}$$

Equation 21 adjusts the equipment cost and inflation variations according to chemical engineering plant cost index (CEPCI) [46].

$$Cost_{2023} = Cost_{REFyear} \times \frac{CEPCI_{2023}}{CEPCI_{REFyear}} \tag{21}$$

where $Cost_{2023}$ represents the average material inflation-adjusted cost for the year 2023, while $Cost_{REFyear}$ denotes the material cost for the specific year under consideration. *CEPCI* serves as the index used to scale the material cost in 2023, based on the index value for material in the year of publication ($CEPCI_{REFyear}$). As defined in Eq. 22, the payback is influenced by annual income and expenditure. The total spending encompasses equipment capital, installation labor, operational yearly workforce, and maintenance costs, whereas the income comprises the total value of both thermal and electrical energy production.

$$Payback(years) = \frac{C_{Components} + C_{Labour} + AnnualC_{Opex} + AnnualC_{Maint}}{Annual\left(\dot{W}_T - \dot{W}_P + \dot{H}_{recovery}\right)} \tag{22}$$

In the thermodynamic and economic analyses, the following assumptions were made:

- The ambient temperature was set as the annual average temperature for Ghaziabad, India (25.7 °C) [47].

Table 4 The variation limits of primary component sizing provided to the optimizer

	Component	Parameter	Min value	Initial value	Max value	Unit
1	Pump	Displacement volume	64	80	100	cm^3
2	Boiler	Heat transfer area	80	100	125	m^2
3	Turbine	Displacement	104	130	162	cm^3
4	Condenser	Heat transfer area	144	180	225	m^2
5	Recuperator	Heat transfer area	150	120	180	m^2
6	APH 1–5	Heat exchange area	225	300	375	m^2
7	Thermal mass 1–3	Mass	1	10000	10000	kg

Table 5 Setup parameters for the NLPQL algorithm

Parameter	Value
Relative gradient step size for finite difference	0.0001
Desired final accuracy	0.00001
Number of iterations	Not limited

- The volumetric and isentropic efficiencies of the pumps were assumed to be 50% and 65%, respectively [48].
- The boiler efficiency was 82%, while the fuel ash content was below 1.7% [49].
- The loss models of Craig & Cox and Moustapha et al. were used to factor in the varying turbine efficiency in design and off-design conditions [49, 50].
- For simplicity, generator efficiency, gearbox efficiency, turbine bearing losses and pump and turbine's working fluid gland leakage were omitted.
- The assumed cooling water pump isentropic efficiency was based on actual operating data was 65%.
- 8000 yearly hours was considered for ORC operation [27].

3.3 Optimization algorithm

As the study concerns capturing waste heat, maximising the output power, rather than cycle efficiency, defined the thermodynamic objective function, Eq. 23. The components' sizing was globally optimized using the NLPQL optimization, utilizing the parameters populated in Table 4. The values in Table 4 were determined based on multiple preliminary iterations, which identified the most effective weighted sum combined both objectives, as in Eq. 22. The optimization initial trial values were determined from a preliminary parametric optimization.

$$ThermodynamicObjective : Max(MeanPower)$$

$$MeanPower = f\left(\begin{array}{c} cycle\ configuration, fluid\ enthalpy, fluid\ superheat, degree\ of\ recuperation, \\ degree\ of\ regeneration, thermal\ mass, APH\ Heat\ transfer \end{array}\right) \tag{23}$$

The economic objective comprises individual objectives in a unified multi-objective function using the weighted sum method [50]. This approach allowed for a more practical techno-economic comparison of ORC. The constraints and weighing in the objective functions were determined through iterative processes to enable the objectives to progress simultaneously [50]. The optimization outcomes and the trade-offs between individual objectives were showcased on a Pareto front to show. Equation 24 governs the weighted sum unified function, with 20% allocated to maximizing the mean power generation and 80% allocated to minimizing the *SIC*. This allocation ensured that the operations are large enough to generate substantial savings and reduce the reliance on human resources, which aligns with the conclusions of prior research [51].

$$F_{weighted\ sum} = \sum 0.8 \times F(SIC) + 0.2 \times F\left(\frac{1}{Mean\ Power}\right) \tag{24}$$

NLPQL applies the linearization of constraints and the Lagrangian function's quadratic approximation to solve continuous differentiable objective functions sequentially [26, 52]. The optimization algorithm uses the criterion by Karush

Table 6 Validation results of conventional ORC with the results of Maraver et al. [20]

Parameter	[20]	Present model	Deviation [%]
Cycle efficiency (%)	10.43	10.28	1.43
Turbine exhaust temperature (°C)	73.9	73.5	0.54
Turbine exhaust specific entropy (J/kg K)	1830	1881	2.78

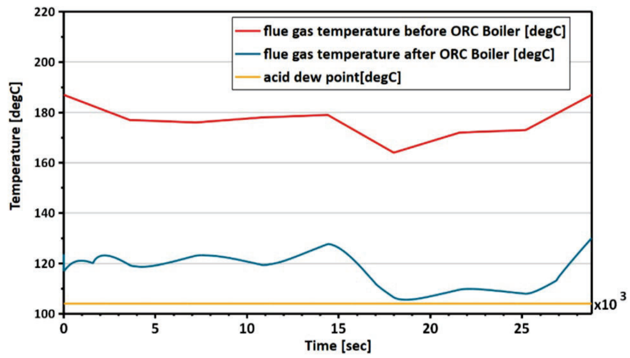

Fig. 5 Flue gas temperatures across the boiler

Kuhn Tucker (KKT) to solve nonlinear equations by performing a first-order derivative test [53]. Equation 25 defines the finite difference calculation of the relative gradient steps, where the relative gradient step is denoted by (δ) [54]. Table 5 details the parameters for implementing NLPQL optimization for the cycle configurations.

$$\overline{grad}(f)(x_0, y_0) = \begin{pmatrix} \frac{\delta f}{\delta x(x_0, y_0)} \\ \frac{\delta f}{\delta y(x_0, y_0)} \end{pmatrix} = \begin{pmatrix} \frac{f(x_0, y_0) - f(x_0 + \delta x_0, y_0)}{(\delta x_0)} \\ \frac{f(x_0, y_0) - f(x_0, y_0 + \delta y_0)}{(\delta y_0)} \end{pmatrix} \quad (25)$$

3.4 Model validation

Previous research by Maraver et al. was used as a benchmark to validate the computational model of the baseline ORC utilizing R245fa and steady heat source at 170 °C without heat recovery [20]. 10–20 °C was the range of heat sink's temperature gradient, while the condenser's temperature was maintained at 35 °C. 115 °C working fluid temperature with a degree of superheating of at least 5 °C corresponding to 14.6 bar evaporator pressure was observed. The boiler and condenser heat exchangers' minimum pinch point were maintained at 10 °C and the condenser subcooling degree was maintained at 5 °C. Table 6 reports the deviations between the results of the present model and reference [20].

4 Results and discussion

4.1 Analysing the optimized cycles

The steam boiler in the presented case study (i.e., textile plant) operates continuously. As shown in Fig. 5, the heat exchangers maintained their temperature above the condensation temperature of acid content in the flue gas to minimise the chances of corrosion.

In Fig. 6, the power output of the optimized cycles is compared to the baseline ORC. Recuperation increased the cycle's power output by 7.53 kW from 49.97 and improved efficiency by 0.81% from 5.16. The combination of a high level of recuperation (C-5) with thermal mass integration led to the system's second-best performance, increasing power output by 14.1%, despite a 1.1% decrease because of thermal mass integration (C-1). However, the incorporation of regeneration affected the power output, consistent with a previous study by Xi et al. [22]. Regenerative cycles reduced the power output by low-pressure turbine (LPT) and the LPT flow rate, in line with Feng et al. [55].

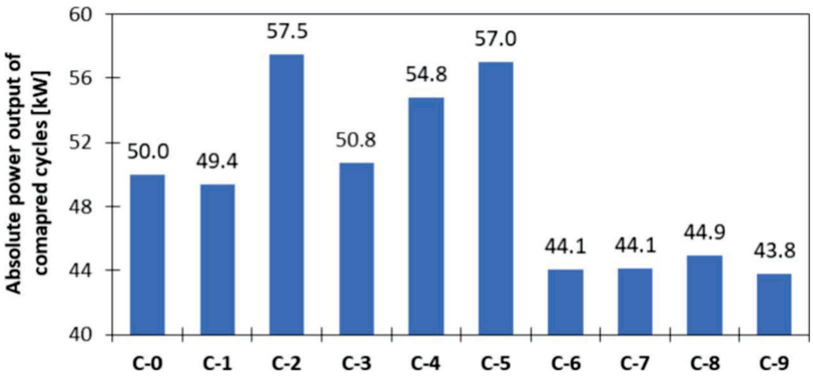

Fig. 6 Parametrically optimized ORCs—absolute power output

Cycle name	Configuration	Cycle name	Configuration
C-0	Baseline	C-5	Recuperation & Thermal mass
C-1	Thermal mass	C-6	Regeneration & air preheating
C-2	With recuperation	C-7	Regeneration
C-3	With air preheating	C-8	Regeneration & Recuperation
C-4	Recuperation & air preheating	C-9	Regeneration & Thermal mass

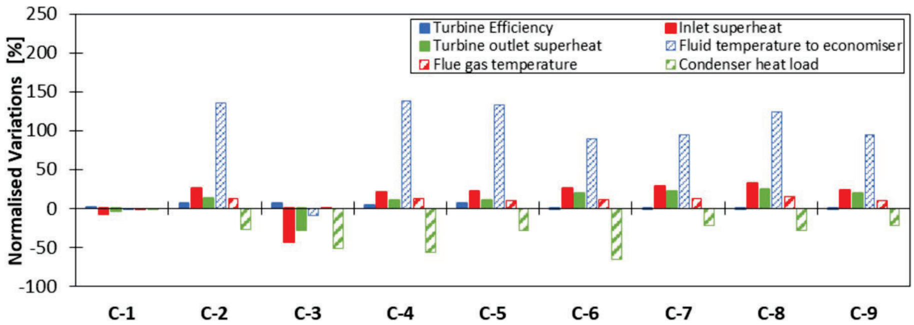

Fig. 7 The variation compared to a conventional cycle of mean turbine isentropic efficiency, turbine inlet degree of superheat, turbine outlet degree of superheat, fluid temperature inlet to economiser, flue gas temperature and condenser heat load for the parametrically optimized ORC configurations

Figure 7 illustrates the variations in the normalized mean turbine isentropic efficiency, turbine inlet and outlet degree of superheat, fluid temperature at the inlet to the economizer, flue gas temperature, and condenser heat load in the parametrically optimized ORCs. The investigation revealed a maximum 7% variation in efficiency across the ORC configurations, emphasizing the significance of turbine efficiency in evaluating cycle-level performance. ORCs with regeneration exhibited the least isentropic efficiency of 84.5%, aligning with Mago et al. [23]. The study considered the mean isentropic efficiency of turbines in ORCs with regeneration. The decrease in isentropic efficiency in regenerative cycles was attributed to a low $\frac{U}{C_2}$ ratio, representing the ratio between turbine wheel tip speed and spouting velocity. The reduced flow rate in the LP turbine increased secondary loss, which could be mitigated by reducing the turbine diameter and lowering blade pitch velocity (U) to minimize secondary loss by increasing blade heights. Conversely, cycles incorporating recuperation exhibited up to 91% isentropic efficiencies, the height.

The baseline cycle had an absolute superheat of 23.48 °C at the turbine inlet, while other configurations ranged between 13.27 and 31.1 °C. At the turbine outlet, the conventional cycle had an absolute superheat of 47.76°C, while other cycles varied between 34.8 and 58.4 °C. The recuperative and regenerative cycles showed elevated inlet superheat temperatures because of the heat recovery. However, in cycles incorporating regenerative, the exit superheat was the highest because of the turbines' inferior isentropic efficiency. The cycles incorporating the preheater exhibited the lowest average superheat at the into the turbine. This was attributed to the heat removed by the preheater, as evidenced by the increased pump's discharge sub-cooling—36.8 °C for the ORC incorporating preheater and 22.6 °C for the baseline ORC.

The baseline ORC could not function during preheating, but at 38.6 °C saturation temperature. However, the working fluid temperature was notably elevated in the cycles incorporated recuperation and regeneration. Although the thermal mass stored heat, it did not enhance the fluid temperature.

Increasing the working fluid's temperature decreases the heat transfer across the boiler. Such an increase in the temperature of flue gas maintains the energy balance but negatively impacts the efficiency of the heat recovery cycles. In the

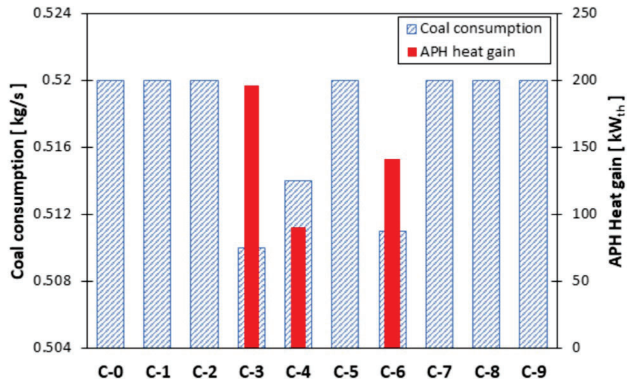

Fig. 8 Fuel consumption and heat gain by incorporating preheaters

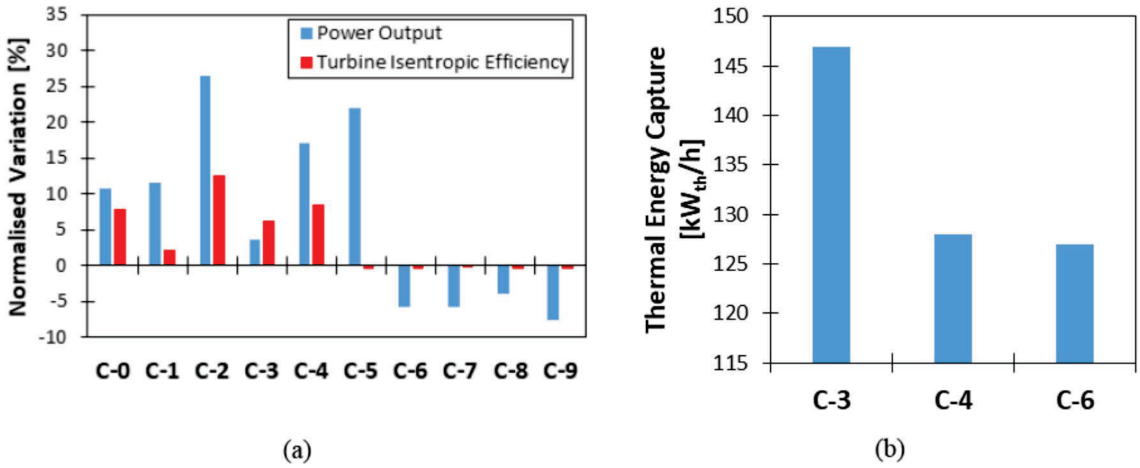

Fig. 9 **a** Normalised power output gains turbine isentropic efficiency variation; **b** Thermal Energy Capture

baseline ORC with 308 kW-th capacity, 108 m3/h cooling water flow was utilized to match the average cooling demand. However, this resulted in 6.5 m^3/h loss of water vapor in the wet cooling tower [56].

This study explored three distinct methods for lowering the condenser's heat load. The first approach involved implementing a regenerative cycle, reducing the condenser flow [22]. The second method reduces the enthalpy through indirect heat exchange employing recuperation. Last, low-grade heat was extracted to preheat air in the steam boiler cycle. Because of the regenerative cycle's lower the working fluid's condensation rate, the heat load in the condenser in C-7 was reduced by approximately 20%.

By utilizing the C-2 recuperative cycle, the condenser heat rejection was decreased by 28%, directly related to the extent of recuperation. When the turbine exit working sensible heat is reduced, incorporating air preheating in C-3, 4, and 6 resulted in the lowest condenser heat loads. By reducing the heat load, the finite-sized condenser could lower the average condenser pressure to 2.01 bar, compared to the baseline ORC's 2.30 bar. The heat load in the C-3's condenser with air preheating was approximately 50% less than that of the baseline ORC. The C-6 showed the highest heat rejection reduction of 65% in condenser results from reducing sensible heat removed from the condenser. Combining the air preheating and recuperation in C-4 showed a 57% less heat load in the condenser.

Integrating the air preheater is beneficial for harnessing the waste heat from the ORC within an established industrial process. A notable decrease of 1.9% in boiler fuel consumption, 1.16%, and 1.66% was observed in C-3, C-4, and C-6, respectively, agreeing with Chao et al. [57]. Figure 8 depicts the average heat recovered by incorporating APH and their corresponding average fuel consumption. Incorporating the APH into a conventional cycle yielded the highest average heat recovered by 196 kW-th.

Fuel savings enabled cost benefits by reducing equipment size, fuel logistics, flue gas treatment (e.g., desulfurization), and air pollution. Previous research has quantified the CO2 emissions at 2.62 tons per ton of coal [57], indicating that combustion waste heat recovery also has environmental benefits such as reducing particulate matter, lowering carbon footprint, and minimizing ash discharge.

Table 7 Optimized component sizes provided

Component	Unit	Cycle				
		(C-0)	(C-1)	(C-2)	(C-3)	(C-4)
Pump displacement	cm^3	89	95	91	79	88
Boiler area	m^2	103	90	120	120	120
Turbine displacement	cm^3	104	104	104	104	104
Condenser area	m^2	215	214	216	216	216
Recuperator area	m^2	–	–	180	–	143
Cycle	unit	(C-5)	(C-6)	(C-7)	(C-8)	(C-9)
Pump displacement	cm^3	88	94	96	93	91
Boiler area	m^2	119	119	112	118	100
Turbine displacement	cm^3	111	105	128	113	124
Condenser area	m^2	216	213	199	216	204
Recuperator area	m^2	161	–	–	150	–

Table 8 Material cost of equipment before optimization

Component	Cost in Euros (€)	Component	Cost in Euros (€)
Pump	317	Working fluid	10480
Boiler	17240	Recuperator	24714
Turbine	341	APH	46690
Condenser	70832	Thermal Mass	9600
Piping	6500		

4.2 Thermodynamic optimisation

The optimized conventional ORC configuration resulted in a 5 kWe (10%) increase in power output. The cycle efficiency improved by 12% in the substantial recuperative cycle and 2% by incorporating air preheater. Compared to the parametrically optimized baseline cycle, the substantial recuperative cycle achieved a significant 26.5% improvement, with the efficiency enhancement directly proportionate to the degree of recuperation.

Power output improvement was observed in C-1, 2, 4, and 5, with the normalized gains shown in Fig. 9a. The overall power generation was found to have a strong correlation with the mean turbine isentropic efficiency, emphasizing the importance of turbine performance in optimizing the cycle performance. The optimized component sizes are furnished in Table 7, where the variation of component sizes is attributed to the differing global and local optimization approaches, a key aspect of this research.

With the singular objective of enhancing the output power, the optimized cycles did not enhance the heat recovery for cycles incorporating air preheaters, as depicted in Fig. 9b. This optimization for power output led to a decrease in heat recovery by up to 24%. However, the recuperative cycle incorporated air preheater showed a reassuringly balanced approach, maximizing both electrical and heat recovery.

4.3 Multi-objective optimization

Table 8 displays the initial costs of major components before any optimization, which aligns with the findings of Shengjun et al. [58], who concluded that heat exchangers account for 80–90% of traditional ORC expenses. Before optimization, 44,842 €/kW specific investment cost was observed. Following optimization, 2122 €/kW the baseline ORC's cost per unit of installed capacity was determined, consistent with 1800–2500 €/kW determined by Astolfi et al. [59].

For most configurations, the optimization significantly improved the identified objectives towards the predefined goal, resulting in an approximate 1.98% objective enhancement. As shown in Table 9, the optimization algorithm enabled a 26.95% objective enhancement, improving SIC by 21.72%, but the power generation decreased by 1.1% compared to

Table 9 Improvement in composited objective function and SIC values achieved by optimization

	Optimizer	Composite objective function [-]	Composite objective function improvement to original [%]	Composite objective function improvement within cycle [%]	SIC [€/kW]	SIC improvement to original [%]	SIC improvement within cycle [%]	Mean power [kW]	Mean power improvement to original [%]	Mean power improvement within cycle [%]
Conventional ORC	Non-optimized	13682	–	–	18229	–	–	49.97	–	–
	Optimized	9954.8	27.3	27.3	14774	18.9	18.9	50.83	1.7	1.7
Recuperation	Non-optimized	14349	−4.9	–	19581	−7.4	–	57.5	15.1	–
	Optimized	9752.2	28.7	32.0	14789	18.9	24.5	55.35	10.8	−3.7
Recuperation + APH	Non-optimized	8638	36.9	–	13623	25.3		54.78	9.6	
	Optimized	6993.4	48.9	19.0	12063	33.8	11.5	55.71	11.5	1.7
APH	Non-optimized	7075.2	48.3		11445	37.2	–	48.02	−3.9	–
	Optimized	4892.5	64.2	30.9	9235	49.3	19.3	47.72	−4.5	−0.6
Recuperation + Thermal Mass	Non-optimized	11486	−5.9	–	19769	−8.4	–	58.05	16.2	–
	Optimized	9780.7	28.5	32.5	15046	17.5	23.9	57.86	15.8	−0.3
Regeneration + APH	Non-optimized	8386.1	38.7	–	12886	29.3	–	49.45	−1.0	–
	Optimized	6976.2	49.0	16.8	11245	38.3	12.7	46.91	−6.1	−5.1

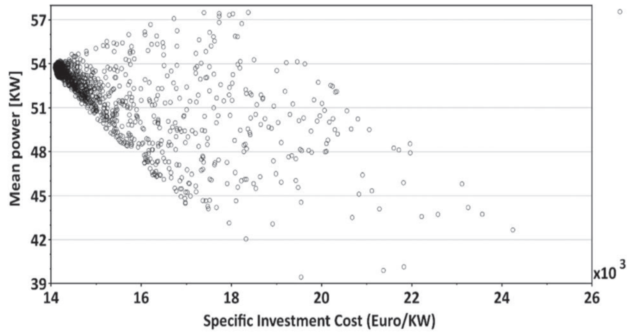

Fig. 10 NLPQL-optimized baseline ORC cycle represented on Pareto front—mean power and specific cost investment compound objective

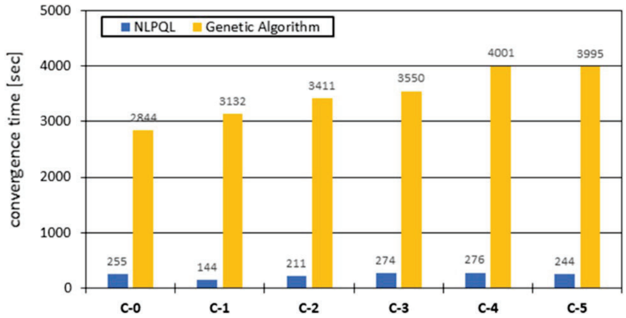

Fig. 11 Comparing the computational intensity for NLPQL and Genetic Algorithm

Table 10 The sizes of the main components resulted from multi-objective optimization

Cycle	Pump displacement	Boiler area	Turbine displacement	Condenser area	Recuperator area	APH area	Thermal mass
Unit	cm^3	m^2	cm^3	m^2	m^2	m^2	kg
Conventional ORC	77.8	75.0	98.0	143.1	–	–	–
Recuperation	94.65	79.2	98.10	135	180	–	–
Recuperation + APH	78.24	125.0	126.55	135	143	354	–
APH	77.78	109.0	130.8	135	–	225	–
Recuperation + Thermal Mass	91.59	92.93	98.0	135	144.42	–	31976
Regeneration + APH	97.63	117.34	113.6	135	–	296.5	–

the unoptimized baseline ORC. Additionally, there is an up to 8.6% reduction in power output in cycles incorporating air preheater while achieving up to a 30.9% objective improvement. The cycle incorporated air preheating showed the most SIC improvement of 49.3% compared to the baseline ORC, with only a 4.5% reduction in power. This trend was also evidence in the Pareto front, depicted in Fig. 10, illustrating a discernible trade-off between both objectives. The unified objective was comprehensive to determine the best overall configuration.

It is noteworthy that an initial investigation compared NLPQL to the commonly known Genetic for the investigated configurations. It can be observed that the former enabled highly credible optimisation at low computational cost, as shown in Fig. 11.

The payback results from the optimized ORC incorporating air preheating, considering an 8% annual interest rate and 1% of capital cost as annual maintenance cost [60]. ORCs do not cause extensive human resources; they are closed loops and can be automatically controlled [27]. The analysis included 5 h of preventive maintenance per week at a rate of 30 €/hr per operator [12, 61]. Accordingly, 1.72 years payback period was determined. Table 10 outlines the sizes of the main ORC components determined from optimization process.

5 Conclusions

This study aimed to conduct multi-objective optimization of the component sizes for ORCs of different cycle configurations. The specific objectives were to minimize the specific investment cost while maximizing the power output when utilising unsteady heat source while wasted from a process industry. The study's conclusions are as follows.

- The highest power output was achieved by the recuperative cycle, surpassing the baseline cycle by 15%. In contrast, cycles that integrated regeneration demonstrated no enhancement in electrical power generation.
- Investigating ORC configurations revealed a variation of up to 7% in the turbine's isentropic efficiency, highlighting the significance of considering the variability in isentropic efficiency.
- The Air Preheater reduced the heat load on the condenser and enabled 195 kWth heat recovery, resulting in up to 1.9% environmental benefits and reduced fossil fuel consumption.
- Although the enhance power generation was not notably enhanced by utilizing, its capacity to mitigate abrupt changes in heat sources was evidenced.
- Combining regeneration and recuperation boosted the level of superheating by 32%.

Author contributions Conceptualization, Ahmed Rezk and Mahmoud Elsheniti; data curation, Yohan Engineer, Ahmed Rezk, and Ehsan Baniasadi; formal analysis, Yohan engineer and Ahmed Rezk; investigation, Yohan Engineer and Ahmed Rezk; methodology, Yohan Engineer and Ahmed Rezk; Resources, Ahmed Fouly; software, Yohan Engineer; supervision, Ahmed Rezk; validation, Yohan Engineer; visualization, Mahmoud Elsheniti, Ali Radwan, Ehsan Baniasadi and Ahmed Fouly; writing—original draft, Yohan Engineer; writing—review & editing, Ahmed Rezk and Mahmoud Elsheniti.

Data availability No datasets were generated or analysed during the current study.

Declarations

Competing interests The authors declare no competing interests.

References

1. Meana-Fernández A, et al. Power plant cycles: evolution towards more sustainable and environmentally friendly technologies. Energies. 2022;15(23):8982.
2. Bhaumick A, et al. Performance of compound parabolic collector integrated with organic Rankine cycle under low mass flow rates for clean energy. Int J Environ Sci Technol. 2024. https://doi.org/10.1007/s13762-024-05605-9.
3. Wang L, et al. Multi-objective optimization of an organic Rankine cycle (ORC) for a hybrid solar-waste energy plant. Energies. 2024;17(8):1810.
4. Albaik I, et al. Assessment of a novel multi-generation solar CPV/T system combining adsorption and organic Rankine cycle subsystems. Sol Energy. 2022;236:455–72.
5. Başoğul Y. A parametric study on exergoeconomic analysis for a binary geothermal power plant with ORC. Int J Green Energy. 2021;18(11):1117–28.
6. Maali R, Khir T, Arici M. Energy and exergy optimization of a combined solar/geothermal organic Rankine cycle power plant. J Cent South Univ. 2023;30(11):3601–16.
7. Marenco-Porto CA, et al. Evaluation of organic Rankine cycle alternatives for the cement industry using Analytic Hierarchy Process (AHP) methodology and energy-economic-environmental (3E) analysis. Energy. 2023;281:128304.

8. Xue K, et al. Energy and exergy analysis of waste heat recovery from pressurized hot smothering steel slag by solar organic Rankine cycle. J Therm Anal Calorim. 2023;148(19):10241–50.
9. Mana AA, et al. Enhancing sustainable energy conversion: comparative study of superheated and recuperative ORC systems for waste heat recovery and geothermal applications, with focus on 4E performance. Energy. 2023;284:128654.
10. Lecompte S, et al. Review of organic Rankine cycle (ORC) architectures for waste heat recovery. Renew Sustain Energy Rev. 2015;47:448–61.
11. Park B-S, et al. Review of organic Rankine cycle experimental data trends. Energy Convers Manage. 2018;173:679–91.
12. Campana F, et al. ORC waste heat recovery in European energy intensive industries: energy and GHG savings. Energy Convers Manage. 2013;76:244–52.
13. Forman C, et al. Estimating the global waste heat potential. Renew Sustain Energy Rev. 2016;57:1568–79.
14. Ohijeagbon IO, Waheed MA, Jekayinfa SO. Methodology for the physical and chemical exergetic analysis of steam boilers. Energy. 2013;53:153–64.
15. Braimakis K, Charalampidis A, Karellas S. Techno-economic assessment of a small-scale biomass ORC-CHP for district heating. Energy Convers Manage. 2021;247:114705.
16. Arsie I, et al. A new generation of hydrogen-fueled hybrid propulsion systems for the urban mobility of the future. Energies. 2024;17(1):34.
17. Bao J, Zhao L. A review of working fluid and expander selections for organic Rankine cycle. Renew Sustain Energy Rev. 2013;24:325–42.
18. Méndez-Cruz LE, et al. Thermodynamic optimization of trigeneration power system. Energies. 2024;17(12):3048.
19. Guo C, et al. Organic Rankine cycle for power recovery of exhaust flue gas. Appl Therm Eng. 2015;75:135–44.
20. Maraver D, et al. Systematic optimization of subcritical and transcritical organic Rankine cycles (ORCs) constrained by technical parameters in multiple applications. Appl Energy. 2014;117:11–29.
21. Labbe DE, ME Brown Jr. Attemperator-deaerator condenser. 1983, Google Patents.
22. Xi H, et al. Parametric optimization of regenerative organic Rankine cycle (ORC) for low grade waste heat recovery using genetic algorithm. Energy. 2013;58:473–82.
23. Mago PJ, et al. An examination of regenerative organic Rankine cycles using dry fluids. Appl Therm Eng. 2008;28(8–9):998–1007.
24. Di Battista D, et al. On the limiting factors of the waste heat recovery via ORC-based power units for on-the-road transportation sector. Energy Convers Manage. 2018;155:68–77.
25. Roumpedakis TC, et al. Exergetic and economic analysis of a solar driven small scale ORC. Renewable Energy. 2020;157:1008–24.
26. Hu N, Zhou P, Yang J. Comparison and combination of NLPQL and MOGA algorithms for a marine medium-speed diesel engine optimisation. Energy Convers Manag. 2017;133:138–52.
27. Wang X-Q, et al. Payback period estimation and parameter optimization of subcritical organic Rankine cycle system for waste heat recovery. Energy. 2015;88:734–45.
28. Ahmadi SF, et al. Energy management and reducing the environmental impacts of industrial flare gases using a new trigeneration energy system. Process Saf Environ Prot. 2023;177:1129–41.
29. Ebadollahi M, et al. Development of a novel flexible multigeneration energy system for meeting the energy needs of remote areas. Renew Energy. 2022;198:1224–42.
30. Alameer Z, et al. Multistep-ahead forecasting of coal prices using a hybrid deep learning model. Resour Policy. 2020;65:101588.
31. Widodo S, et al. Characterization of some coal deposits quality by use of proximate and sulfur analysis in the Southern Arm Sulawesi, Indonesia. Int J Eng Sci Appl. 2017;3(2):137–43.
32. Mastral AM, et al. Assessment of PAH emissions as a function of coal combustion variables in fluidised bed. 2. Air excess percentage. Fuel. 1998;77(13):1513–6.
33. Rayegan R, Tao YX. A procedure to select working fluids for Solar Organic Rankine Cycles (ORCs). Renew Energy. 2011;36(2):659–70.
34. Craig HRM, Cox HJA. Performance estimation of axial flow turbines. Proc Inst Mech Eng. 1970;185(1):407–24.
35. Moustapha SH, Kacker SC, Tremblay B. An improved incidence losses prediction method for turbine airfoils. J Turbomach. 1990;112(2):267–76.
36. Engineer Y, Rezk A, Hossain AK. Energy analysis and optimization of a small-scale axial flow turbine for Organic Rankine Cycle application. Int J Thermofluids. 2021;12:100119.
37. Lu X, et al. Thermodynamic and dynamic analysis of a hybrid PEMFC-ORC combined heat and power (CHP) system. Energy Convers Manage. 2023;292:117408.
38. Adams TM, Grant C, Watson HD. A simple algorithm to relate measured surface roughness to equivalent sand-grain roughness. Int J Mech Eng Mechatron. 2012. https://doi.org/10.11159/ijmem.2012.008.
39. Braimakis K, Karellas S. Energetic optimization of regenerative Organic Rankine Cycle (ORC) configurations. Energy Convers Manage. 2018;159:353–70.
40. von Helmholtz H, Hittorf JW, Waals JD. Physical memoirs selected and translated from foreign sources. Oxfordshire: Taylor & Francis; 1888.
41. Marler RT, Arora J. Survey of multi-objective optimization methods for engineering. Struct Multidiscip Optim. 2004;26:369–95.
42. Golubev SS, et al. Analysis of the current state and forecast of cast iron production in Russia. Arch Foundry Eng. 2021;21(2):70.
43. Quoilin S, et al. Thermo-economic optimization of waste heat recovery Organic Rankine Cycles. Appl Therm Eng. 2011;31(14–15):2885–93.
44. Lecompte S, et al. Part load based thermo-economic optimization of the Organic Rankine Cycle (ORC) applied to a combined heat and power (CHP) system. Appl Energy. 2013;111:871–81.
45. Kavvadias KC, Quoilin S. Exploiting waste heat potential by long distance heat transmission: design considerations and techno-economic assessment. Appl Energy. 2018;216:452–65.
46. Cost Engineering: Equipment Purchase Costs, in Chemical Engineering. 2018.
47. Indian Meteorological Department (Ministry of Earth Sciences), Government of India. https://mausam.imd.gov.in/imd_latest/contents/index_smart_cities1.php. Accessed 2021.
48. Roy JP, Mishra MK, Misra A. Parametric optimization and performance analysis of a waste heat recovery system using Organic Rankine Cycle. Energy. 2010;35(12):5049–62.
49. Muthuraman M, Namioka T, Yoshikawa K. A comparative study on co-combustion performance of municipal solid waste and Indonesian coal with high ash Indian coal: a thermogravimetric analysis. Fuel Process Technol. 2010;91(5):550–8.

50. Konak A, Coit DW, Smith AE. Multi-objective optimization using genetic algorithms: a tutorial. Reliab Eng Syst Saf. 2006;91(9):992–1007.
51. Marler RT, Arora JS. Survey of multi-objective optimization methods for engineering. Struct Multidiscip Optim. 2004;26(6):369–95.
52. Ayancik F, et al. Simulation-based design and optimization of Francis turbine runners by using multiple types of metamodels. Proc Inst Mech Eng C J Mech Eng Sci. 2017;231(8):1427–44.
53. Schittkowski K. Mathematical programming software. In: Prékopa A, Szelezsáan J, Strazicky B, editors. System modelling and optimization. Berlin: Springer; 1986. p. 804–10.
54. Schittkowski K. Mathematical programming software. Berlin: Springer; 1986.
55. Feng Y, et al. Comparison between regenerative organic Rankine cycle (RORC) and basic organic Rankine cycle (BORC) based on thermoeconomic multi-objective optimization considering exergy efficiency and levelized energy cost (LEC). Energy Convers Manage. 2015;96:58–71.
56. Qureshi BA, Zubair SM. Prediction of evaporation losses in wet cooling towers. Heat Transfer Eng. 2006;27(9):86–92.
57. Chao L, et al. The effect analysis of thermal efficiency and optimal design for boiler system. Energy Procedia. 2017;105:3045–50.
58. Shengjun Z, Huaixin W, Tao G. Performance comparison and parametric optimization of subcritical Organic Rankine Cycle (ORC) and transcritical power cycle system for low-temperature geothermal power generation. Appl Energy. 2011;88(8):2740–54.
59. Astolfi M, et al. Binary ORC (Organic Rankine Cycles) power plants for the exploitation of medium–low temperature geothermal sources–Part B: Techno-economic optimization. Energy. 2014;66:435–46.
60. Bhatt V, Virmani A. Global integration of India's money market: Interest rate parity in India. 2005, Working Paper.
61. Müller T, Schulten T. The European minimum wage on the doorstep. SSRN J. 2020.